Decadal Variations in the Global Atmospheric Land Temperatures

Richard A. Muller[1,2,3], Judith Curry[4], Donald Groom[2],
Robert Jacobsen[1,2], Saul Perlmutter[1,2], Robert Rohde[3],
Arthur Rosenfeld[1,2], Charlotte Wickham[5], Jonathan Wurtele[1,2]

[1] Dept. of Physics, University of California, Berkeley CA 94720; [2]Lawrence Berkeley National Laboratory, Berkeley CA 94720; [3]Novim Group, Berkeley Earth Surface Temperature Project, 211 Rametto Road, Santa Barbara CA 92104 ; [4]Georgia Institute of Technology, Atlanta GA 30332; [5]University of California, Berkeley, now at Dept. of Statistics, Oregon State University. Correspondence for all authors should be sent to The Berkeley Earth Surface Temperature Project, 2831 Garber St., Berkeley CA 94705.

Abstract

Interannual to decadal variations in Earth global temperature estimates have often been identified with El Nino Southern Oscillation (ENSO) events. However, we show that variability on timescales of 2-15 years in mean annual global land surface temperature anomalies T_{avg} are more closely correlated with variability in sea surface temperatures in the North Atlantic. In particular, the cross-correlation of annually-averaged values of T_{avg} with annual values of the AMO, the Atlantic Mutidecadal Oscillation index, is much stronger than the cross-correlation of T_{avg} with ENSO. The pattern of fluctuations in T_{avg} from 1950 to 2010 reflects true climate variability, and is not an artifact of station sampling. A world map of temperature correlations shows that the association with AMO is broadly distributed and unidirectional. The effect of El Nino on temperature is locally stronger, but can be of either sign, leading to less impact on the global average. We identify one strong narrow spectral peak in the AMO at period 9.1 ± 0.4 years and p-value 1.7% (CL 98.3%). Variations in the flow of the Atlantic Meridional Overturning Circulation may be responsible for some of the 2-15 year variability observed in global land temperatures.

1. Introduction

The average earth land surface temperature, T_{avg}, is a key indicator of climate change. Detailed analyses of T_{avg} have been reported by three major teams: the National Oceanographic and Atmospheric Administration (NOAA; see *Menne et al.* [2005]), the NASA Goddard Institute for Space Science (GISS; see *Hansen et al.* [2010]), and a collaboration of the Hadley Centre of the UK Meteorological Office with the Climate Research Unit of East Anglia (HadCRU; see *Jones et al.* [2003], *Brohan et al.* [2005]). Results from their analysis are shown in Figure 1. The time period in the plot is begins at 1950 since a large number of new stations were introduced at that time; the uncertainties prior to 1950 are substantially larger. Note that in this paper we focus of the land-only temperature average – not including oceans – so that the time series will not directly include the ocean data that we will use for our correlation analysis.

Also shown in Figure 1 is a new estimate of the Earth atmospheric land surface temperature that we created from data independent of those used by the other three groups. We obtained this estimate by choosing 2000 sites randomly from a list of approximately 30,964 temperature recording stations world-wide that had not been used by NOAA, GISS, or HadCRU. Each temperature record was adjusted by an additive parameter, one per record, to bring it into a best least-squares fit with the other records; details of this procedure are described *Rohde et al.* [2011]. The statistical techniques used (Kriging) are designed to compensate for sampling biases in station coverage. This permits a random selection of stations to be made without giving excessive weight to heavily sampled regions, such as North America and Europe. No adjustments or corrections were made for

52 systematic effects such as urban heat island warming or change of instrumentation.
53 Despite these limitations, the virtue of this estimate is that it is derived from data
54 independent from those previously used. Because of this, the qualitative agreement with
55 the prior estimates confirms that the fluctuations are true indicators of climate and not
56 artifacts of data selection and processing. The four curves show a broad trend of "global
57 warming" with some unevenness; the lack of warming from 1950 to 1975 has been
58 attributed to a combination of natural and anthropogenic factors, especially the cooling
59 effect of increased aerosol pollution [*Jones et al.*, 2003].
60
61 **Figure 1**. Global land temperature estimates T_{avg}, smoothed by a 12-month moving
62 average. [Full caption at end of paper, as required by editor]
63

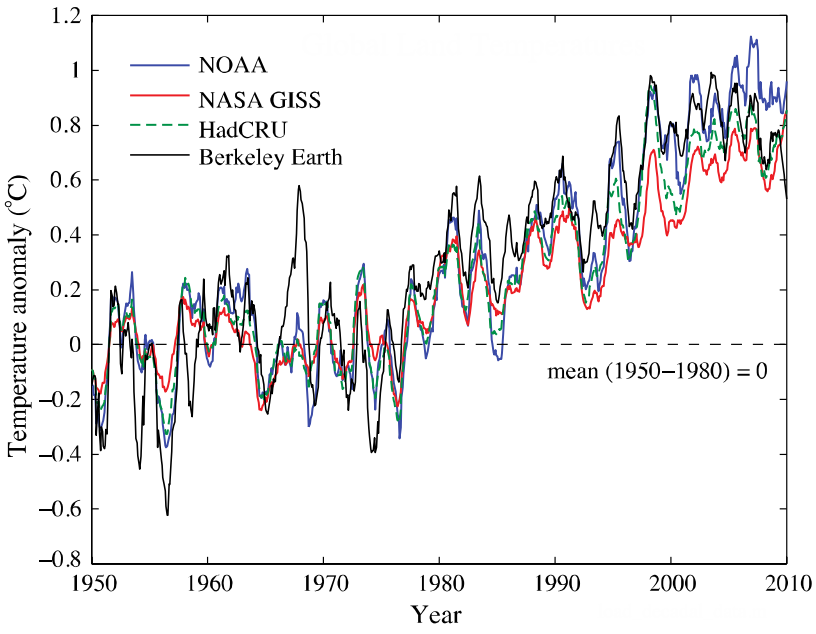

64
65

66 **2. Decadal (2 – 15 yr) Variations**

67

68 Much attention has been given to the small T_{avg} maxima of 1998 and 2005. The maximum
69 in 1998 occurred during a very strong El Nino, and is plausibly associated with that oceanic
70 event [Trenberth, 2002]. In this study we examined the annually-averaged global land
71 temperature time series to study their possible correlation not only with the El Nino
72 Southern Oscillation index (ENSO; see *NOAA* [2005]) but with the Atlantic Multidecadal
73 Oscillation (AMO; see *Schlesinger et al.* [1994] and *Enfield et al.* [2001]), the Pacific
74 Decadal Oscillation (PDO, see *Zhang et al.* [1997]), the North Atlantic Oscillation (NAO,
75 see *Zhang et al.* [1997], *Hurrell et al.* [1995]), and the Arctic Oscillation (AO, see
76 *Thompson et al.* [1998]). Three of these indices: ENSO, AMO, PDO, are derived from sea
77 surface temperature records, in the equatorial Pacific, the North Atlantic, and the North
78 Pacific respectively. Two of these, the NAO and the AO, are derived from surface pressure
79 differences at locations in the northern Atlantic and Arctic. We find that the strongest
80 cross-correlation of the decadal fluctuations in land surface temperature is not with ENSO
81 but with the AMO. The AMO index is plotted in Figure 2.

82

Figure 2. The AMO index.

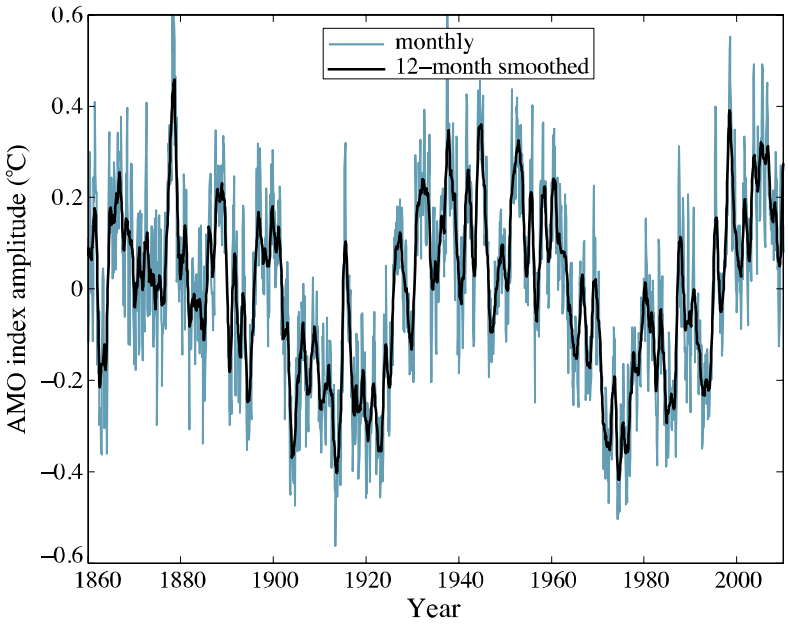

Our analysis used the monthly land-surface average temperature records made available by the four groups previously referenced: NOAA, NASA GISS, HadCRU, and ours, the Berkeley Earth Surface Temperature group. The land temperature data were smoothed with a 12-month running average (boxcar smoothing); this removes high frequency (e.g. monthly) changes. The data prior to 1950 were noisier than the subsequent data, primarily because the number of stations was smaller, and for that reason we restricted the period for our analysis to 1950-2010.

To emphasize the decadal-scale variations, the long-term changes in the temperature records and oceanic indices were "pre-whitened." This is a process to remove a large signal that is not being studied in order to reduce bias in the remainder. To do this, we fit each record (yearly data sets) separately to 5th order polynomials using a linear least-squares regression; we subtracted the respective fits, and normalized the results to unit

mean-square deviation. This procedure effectively removes slow changes such as global warming and the ~70 year cycle of the AMO, and gives each record zero mean. The 12-month smoothing removes high frequency (e.g. monthly) changes. All of the remaining analysis in this paper is based on the pre-whitened temperature records and oceanic indices.

The four temperature estimates after this conditioning are shown in Figure 3A. In 3B and 3C, these four temperature estimates were averaged and compared, in turn, to the conditioned AMO and ENSO. In 3C we directly compare the AMO and ENSO decadal variations.

Figure 3. Decadal fluctuations in surface land temperature estimates and in oceanic indices.

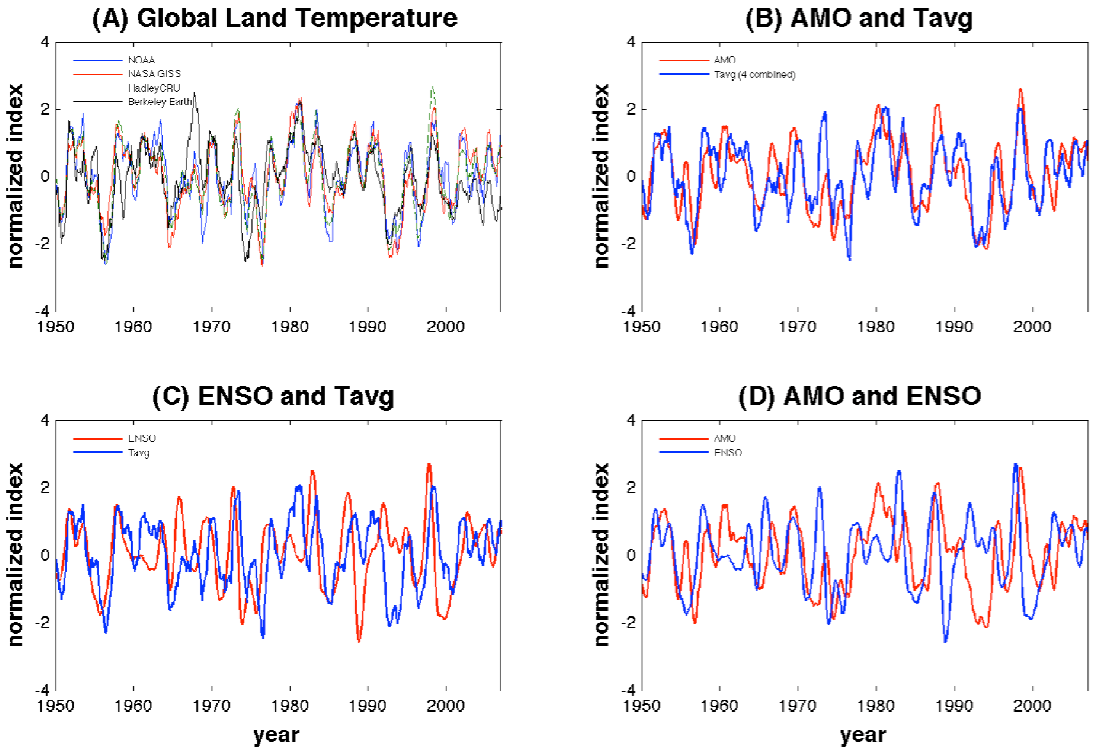

112

113 **3. Difference and Correlation Analysis**

114

115 Visual inspection of Figure 3 suggests that the AMO fluctuations match the temperature
116 variations better than does the ENSO index almost everywhere; perhaps the only prominent
117 exception being 1968 – 1973. This impression is verified by calculating the RMS (root-
118 mean-squared) differences of pairs of plots. The results are shown in Table 1. Note that
119 the RMS of the difference between ENSO and Tavg is over 50% larger than the RMS of
120 the difference between AMO and Tavg. The RMS of the difference between AMO and
121 ENSO is 67% larger than that of AMO and Tavg. The "random" signal, put to show the
122 RMS expected when there is no correlation, was created by breaking the ENSO signal into
123 10 parts and randomly scrambling them; the RMS of the difference between it and the
124 AMO agrees with the theoretical expectation of $\sqrt{2}$.

125

records	RMS
(4 estimates) – Tavg	0.26 C
AMO – Tavg	0.75 C
ENSO – Tavg	1.14 C
AMO – ENSO	1.25 C
AMO - random	1.41 C

126

127 **Table 1.** Root-mean-squared difference of the data shown in Figure 3.
128 The first row shows the RMS deviation of the 4 temperature estimates
129 from Tavg, the average of the four. The other entries show the RMS

deviation of the signal differences. The "random" signal was generated by breaking ENSO into 10 parts and randomly scrambling them in time.

To quantify further the relationship between Tavg and AMO and ENSO, we performed a correlation analysis. Correlation $C(A, B)$ is a measure of the linear time invariant dependence between two time series $\{A(t)\}$ and $\{B(t)\}$. Here, A and B represent either pre-whitened temperature signals or oceanic indices, normalized to zero mean and unit standard deviation. If we include the possibility of a time delay or lag L between the two signals, then we can define the cross-correlation C as

$$C(A, B; L) = \frac{1}{N(L)} \sum A(t)B(t + L)$$

where A and B have zero mean and unit standard deviation and $N(L)$ is the number of terms in the sum. With this definition, the correlation of a function can vary between –1 and +1. At zero lag, the autocorrelation = 1. The value of the correlation at zero lag is commonly called Pearson's Correlation Coefficient, often designated by r.

The correlation estimates between major temperature records and oceanic indices are shown in Figure 4. In these plots, a peak at 0 lag indicates a direct linear correlation between the data sets. A peak offset from zero also indicates correlation but with one lagging the other by the offset.

Figure 4. Decadal correlations of the Berkeley Earth land temperature estimates T_{avg} with the (a) AMO index, (b) ENSO index, (c) PDO index, and (d) NAO index.

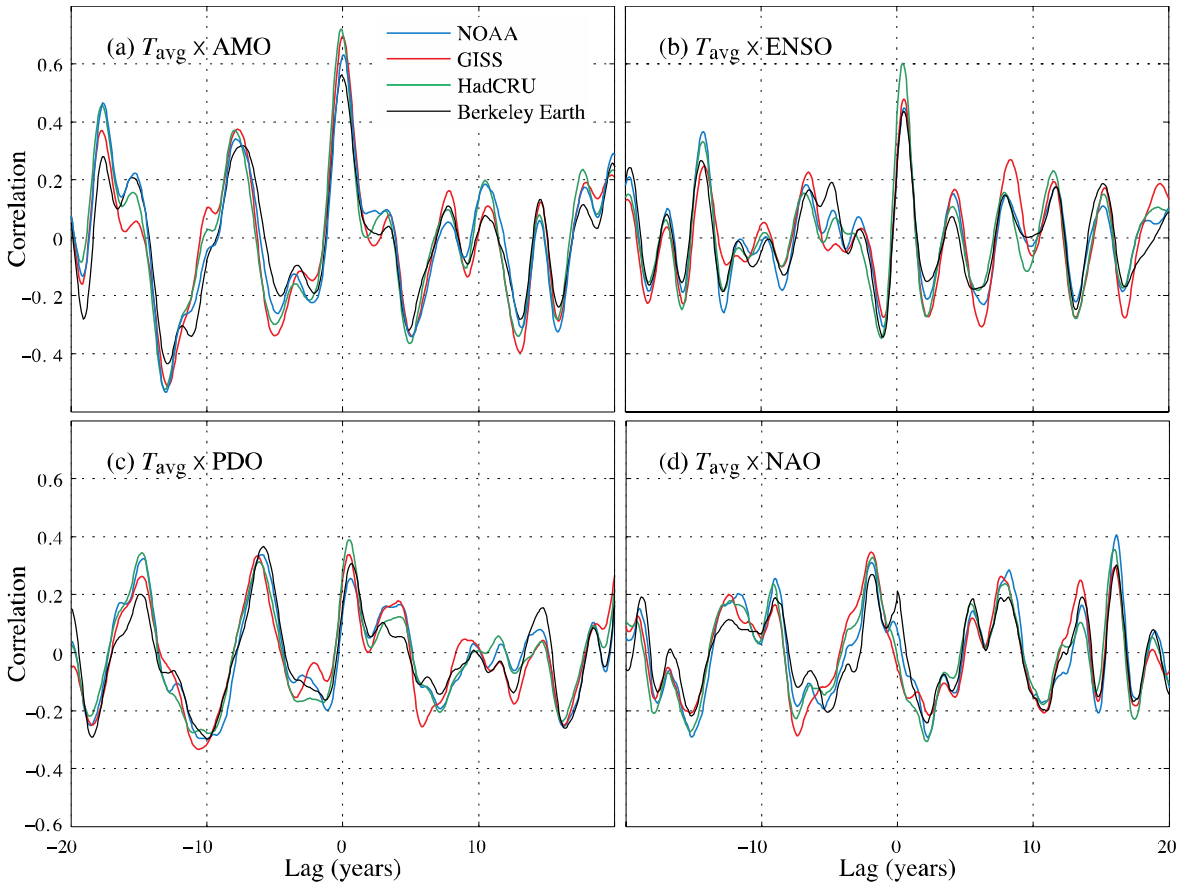

The strongest correlation is observed between the estimates of the average land temperature T_{avg} and AMO, the Atlantic Multidecadal oscillation, with a correlation coefficient $r = 0.65 \pm 0.04$. (In this paper, ± refers to 1 standard error, frequently called by physicists "one standard deviation".) This is the highest peak in any of the cross-correlation plots we calculated, and it occurs at zero lag. The correlation coefficient for the temperature data with ENSO is substantially less, with $r = 0.49 \pm 0.04$. The error uncertainties were estimated from the variance of the four correlations. There is no statistically significant correlation seen in panels (c) and (d).

166 For reference, the maximum correlation between AMO and ENSO in these data is 0.50
167 ± 0.04; with AMO lagging ENSO by 0.70 ± 0.25 years. This is a somewhat larger lag than
168 previously reported 3 months reported in a more detailed analysis of ENSO by *Trenberth et*
169 *al.* [2002].
170
171 To estimate the statistical significance of the AMO *r*-factor, we did a permutation test
172 based on a Monte-Carlo simulation. The AMO pre-whitened record contains 16 points at
173 which the index rises through zero; we chopped the record at these points, creating 17
174 AMO segments. The order of these segments was then permuted randomly and
175 reassembled, creating a simulated AMO. Because of the manner of cutting, the scrambled
176 AMO has many of the same statistical properties as the original AMO; it has the identical
177 amplitude distribution as well as the same number and shapes of peaks and valleys; indeed,
178 it looks to the eye very much like the original AMO. We generated 1,000,000 of these
179 simulated AMOs, and calculated the correlation coefficient *r* for each of these with the T_{avg}
180 of the Berkeley Earth surface land temperature record. In those 1,000,000 simulated AMO
181 trials, the highest value of *r* obtained was 0.49, substantially less than the value of 0.65 ±
182 0.04 obtained with the real AMO, giving a p-factor less than 10^{-6}. Of course, it is not too
183 surprising that land temperature estimates are correlated with sea temperature indices; the
184 key observation is that for interannual to decadal variations, it is the AMO that has the
185 strongest correlation, not ENSO or one of the other indices.
186
187 Figure 5(A) shows the conditioned AMO and PDO indices as a function of time. It can be
188 seen on this plot that PDO generally leads AMO. The correlation is shown in Figure 5(B).
189 Although the correlation peaks near zero lag, the bulk of the central correlation peak is at a

lag of about 2 years. The periodicity of the correlation plot is an indication of a periodicity in both AMO and PDO that we will discuss next.

Figure 5. Correlations between the Atlantic and Pacific Oceanic variability

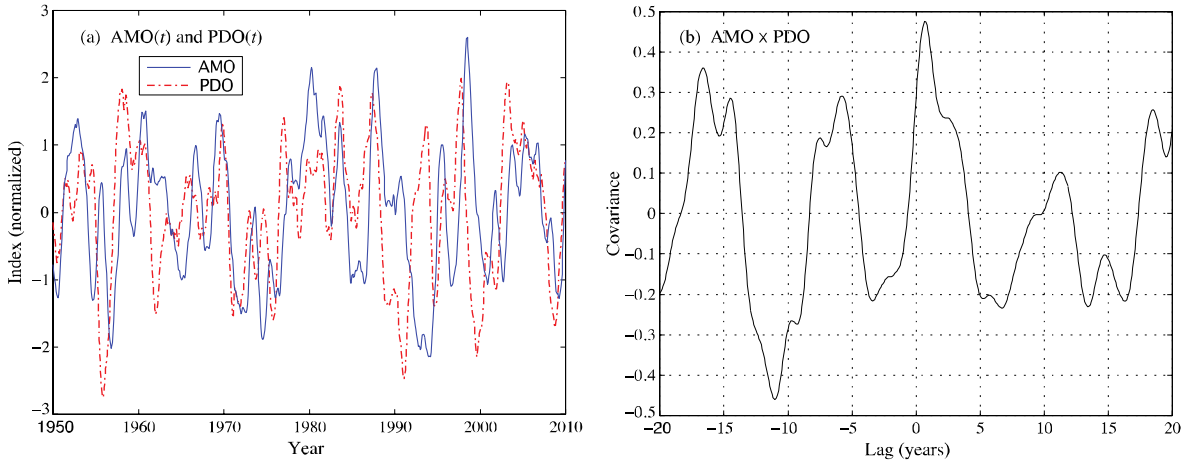

It is not possible from the correlations to ascribe causality with any certainty. For example, Zhang and Delworth [2007] suggested that the observed AMO leads the *inverted* PDO index by about 12 years, and discussed the possible mechanism for the such an Atlantic-Pacific linkage. On our plot Figure 5(b) this corresponds to the large downward variation at Lag of negative 12 years. Such ambiguities could be addressed by mapping the correlation over the world as a function of time.

4. Correlation Map

In Figure 6 we show a map of the decadal correlations both AMO and ENSO with the NOAA global temperature anomaly map; this map includes oceans as well as land. The association with AMO is broadly distributed and unidirectional. The effect of El Nino on

temperature is locally stronger, but can be of either sign, leading to less impact on the global average. The strong correlation of AMO with the Atlantic is of course, a result of the fact that the AMO is derived from Atlantic temperatures; similarly for the strong correlation between ENSO and the equatorial Pacific. ENSO also shows a strong correlation with the Indian ocean. On the land, the AMO affects Africa, southern Asia, and Canada; ENSO correlates most strongly to the continents in the Southern hemisphere. Note its weak correlation to the Atlantic.

Figure 6. Correlation maps of the filtered AMO and ENSO time series

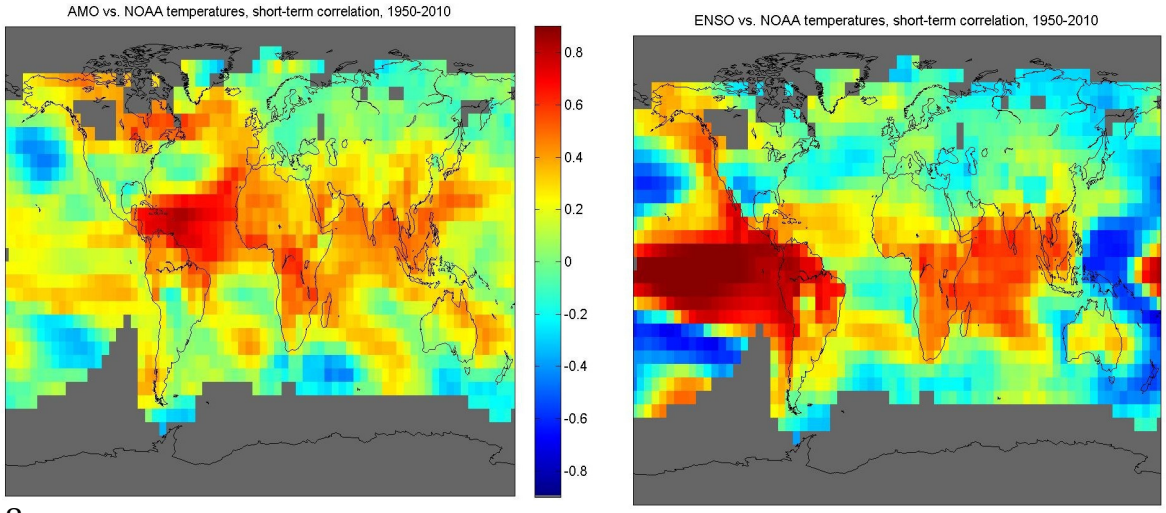

Remarkably, neither AMO nor ENSO shows a strong correlation with the temperature in the United States, although ENSO reaches strongly up the west coast of the US. The variations in the Caribbean, related to the hurricane intensity hitting the southern coast of the US, is more strongly affected by AMO than by ENSO. The correlation patterns help to explain the larger association observed between AMO and Tavg than between ENSO and Tavg. ENSO is locally a more intense effect, but it is also a more complex one giving rise

to both correlated and anti-correlated behavior. By contrast, the AMO map shows positive (or neutral) correlation nearly everywhere. Given this, it is not surprising that the simpler AMO association corresponds to a clearer imprint on the large scale average, Tavg.

5. Spectral Analysis

In Figure 7 we show the spectral power for the AMO and PDO pre-whitened indices. This spectral power estimate is a periodogram, calculated using a Fourier transform with no taper, padded with zeros to yield intermediate frequencies; the spectral method is described in *Muller and MacDonald* [2002].

Figure 7. Spectral power in the (a) Atlantic Multidecadal Oscillation and in (b) the Pacific Decadal Oscillation.

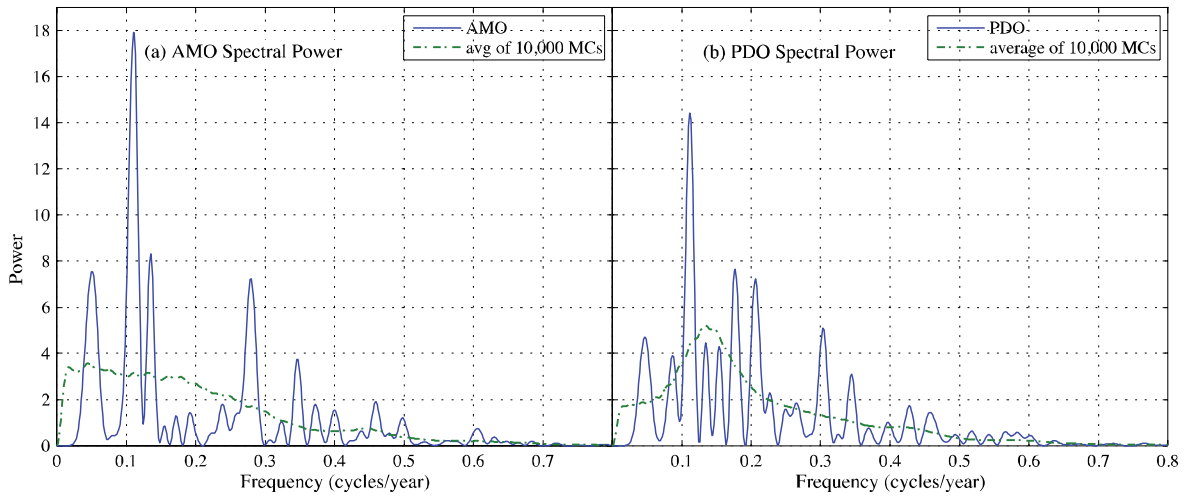

In the AMO spectrum, a strong peak appears at frequency 0.11 ± 0.005 /yr, period 9.1 ± 0.4 years. We place no error bars on this plot because the expected distribution for a power

spectrum is exponential, not gaussian. Instead, we estimate the statistical significance of this peak using the Monte Carlo approach described earlier. 10,000 time-scrambled AMO data were used as estimates of random background. In these runs, we obtained a peak (at any frequency) of spectral power level of 18 or greater a total of 170 times. Based on this, we conclude that probability that the observed peak in the unscrambled data could be due to chance is 170/10,000, i.e. the p-value is 1.7%. For the frequency uncertainty, a cycle of fixed frequency 0.1 cycle/yr and power amplitude 18 (same as the observed peak) was injected into a set of 10,000 scrambled AMO sets, and the observed root-mean-square of the frequency distribution was taken to be the frequency uncertainty.

Although the 9.1 year peak in the AMO has high statistical significance, it contains only 30% of the spectral power; for this reason its presence is not evident to the eye in Figures 3 or 4.

The highest peak in the PDO spectrum, Figure 7 (b) has period 9.0 ± 0.5 years with amplitude 14.4 and p-value 6%. None of the other peaks in Figure 6 are statistically significant. We also looked at the spectra of ENSO, NAO, and Tavg; we did not find any statistically significant narrow spectral signals, although there is of course broad power in the decadal bands.

6. Summary and Discussion

The similarity between the decadal fluctuations in land surface temperature records that use different sources indicates that the fluctuations are physical and not the effect of statistical fluctuations. The 2-15 year variations in AMO, based on sea surface temperature records, strongly correlates with the land record Tavg. Although short-term excursions, such as the temperature maximum in 1998 was widely associated with a strong El Nino event, the AMO is more closely associated with variability in the globally-average land surface temperature than is ENSO.

For a discussion of the variability of the AMO, see *Frankcombe et al.* [2009], who identified important variability in two time scales: 20-30 years, and 50-70 years. In this and much of other analyses prior to ours, the key focus was on longer time scales and so the data were smoothed with a decade-long running average; such a procedure suppresses the interannual to decadal scale variations (2 to 15 year) that are the subject of the present paper.

In the interannual to decadal region we studied, there is only one statistically-significant spectral peak, with period of 9.1 ± 0.4 years, strong in the AMO, weaker in the PDO. It is not present at a statistically significant level in the land T_{avg} or in ENSO or in other ocean indices that we examined. Spectral analysis of global temperatures by others had previously yielded claims of many frequencies, most of which we conclude are not statistically significant when we analyze them using our Monte Carlo background estimation. For example, *Scafetta* [2010], reported a forest of 11 spectral peaks based on a

multitaper analysis; to each of these peaks he calculated 99% confidence intervals. He reported 7 peaks with periods in the range from 5.99 years to 14.8 years. One of these is at our period of 9.1 years; he suggests that this year cycle could be induced by lunar tidal variations. However, we find that when we use our Monte Carlo methods to estimate background, none of his claimed peaks are statistically significant except for the 9.1 year peak; we do not find them in the AMO, PDO, or ENSO.

Correlation does not imply causation. The association between Atlantic sea surface temperature fluctuations and land temperature may simply indicate that both sets of temperatures are responding to the same source of natural variability. However, it is also interesting to consider whether oceanic changes in the AMO may be driving short-term fluctuations in land surface temperature. Such fluctuations might originate as instabilities in the AMO region itself, or they might occur as a non-linear response to changes elsewhere (such as within the ENSO region).

If the fluctuations originate locally, then they might be associated with natural variations in the meridional overturning circulation (MOC) or from salinity anomaly events (Dickson et al., 1988; Belkin,2004). They could be related to a larger instability in the flow of the thermohaline circulation (the oceanic conveyor belt). Computer simulations of the thermohaline circulation by *Jungclaus et al.* [2010] "show pronounced multidecadal fluctuations of the Atlantic overturning circulation and the associated meridional heat transport. The period of the oscillations is about 70–80 yr. The low-frequency variability of the meridional overturning circulation (MOC) contributes substantially to sea surface temperature and sea ice fluctuations in the North Atlantic."

A theory for decadal oscillations in the North Pacific was devised by Munnich [1998]. It involves an interaction between wind and the thermohaline circulation. Such models predict broad spectrum of frequencies, and could drive the structure we see in Figure 3(A), but we would not expect such a driving force to result in the narrow 9.1 yr peak. For more on exited internal modes, see *Frankcombe et al.* [2010] and *Sévellec et al.* [2009, 2010] and the references therein.

Given that the 2-15 year variations in world temperature are so closely linked to the AMO raises (or re-raises) an important ancillary issue: to what extent does the 65-70 year cycle in AMO contribute to the global average temperature change? (*Enfield,* 2006; *Zhang et al.,* 2007; *Kerr*, 1984.) Since 1975, the AMO has shown a gradual but steady rise from -0.35 C to +0.2 C (see Figure 2), a change of 0.55 C. During this same time, the land-average temperature has increased about 0.8 C. Such changes may be independent responses to a common forcing (e.g. greenhouse gases); however, it is also possible that some of the land warming is a direct response to changes in the AMO region. If the long-term AMO changes have been driven by greenhouse gases then the AMO region may serve as a positive feedback that amplifies the effect of greenhouse gas forcing over land. On the other hand, some of the long-term change in the AMO could be driven by natural variability, e.g. fluctuations in thermohaline flow. In that case the human component of global warming may be somewhat overestimated.

In conclusion, our analysis suggests that strong interannual and decadal variations observed in the average land surface temperature records represent a true climate

phenomenon, not only during the years when fluctuations on the timescale of 2-15 years had been previously identified with El Nino events. The variations are strongly correlated with the similar decadal fluctuations observed in the Atlantic Multidecadal Oscillation index, and less so with the El Nino Southern Oscillation index. This correlation could indicate that the AMO plays an important intermediary role in the influence of the Pacific ENSO on world climate; alternatively, it might indicate that variability in the thermohaline flow plays a bigger role than had previously been recognized. The models could be tested by studying the temperature correlations in the ocean as a function of location and time. A 9.1 ± 0.4 year cycle is observed in the pre-whitened AMO, but it contributes only 30% to the variance. A similar cycle at 9.0 ± 0.5 years is seen in the PDO.

7. Acknowledgments

This work was done as part of the Berkeley Earth project, organized under the auspices of the Novim Group (www.Novim.org). We thank many organizations for their support, including the Lee and Juliet Folger Fund, the Lawrence Berkeley National Laboratory, the William K. Bowes Jr. Foundation, the Fund for Innovative Climate and Energy Research (created by Bill Gates), the Ann and Gordon Getty Foundation, by the Charles G. Koch Charitable Foundation, and three private individuals (M.D., N.G. and M.D.). More information on the Berkeley Earth project can be found at www.BerkeleyEarth.org.

360 **8. References**

361

362 Belkin, I.M. (2004), Propagation of the "Great Salinity Anomaly" of the 1990s around the
363 northern North Atlantic. Geophys. Res. Lett., 31, L08306.
364 Brohan, P., J. J. Kennedy, I. Harris, S. F. B. Tett & P. D. Jones (2005), Uncertainty
365 estimates in regional and global observed temperature changes: a new dataset from
366 1850, J. Geophys. Res. 111, D12106, soi:10.1029/2005JD006548. Temperature
367 data are available at:
368 http://hadobs.metoffice.com/hadcrut3/diagnostics/comparison.html
369 Dickson, R. R., Meincke, J., Malmber, S. A. & Lee, A. J. (1988), The ''great salinity
370 anomaly'' in the northern North Atlantic 1968–1982. Prog. Oceanogr. 20, 103–151.
371 Enfield, D.B., A.M. Mestas-Nunez, and P.J. Trimble (2001), The Atlantic Multidecadal
372 Oscillation and its relationship to rainfall and river flows in the continental U.S.,
373 Geophys. Res. Lett., 28: 2077-2080.
374 Frankcombe, L. M., A. von der Heydt and H. A. Dijkstra (2010) North Atlantic
375 Multidecadal Climate Variability: An investigation of dominant time scales and
376 processes, J. Climate, 23, 3626–3638, available at
377 www.phys.uu.nl/~heydt/Publications/Frankcombe-etal-2010.pdf
378 Hansen, J., R. Ruedy, Mki. Sato, and K. Lo (2010), Global surface temperature change.
379 Rev. Geophys., 48, RG4004, doi:10.1029/2010RG000345. Updated Land
380 Temperature data available at: data.giss.nasa.gov/gistemp/graphs/
381 Hurrell, J.W., (1995) Decadal trends in the North Atlantic Oscillation and relationships to
382 regional temperature and precipitation. Science 269, 676-679.

383 Jones, P.D., Jónsson, T. and Wheeler, D. (1997), Extension to the North Atlantic
384 Oscillation using early instrumental pressure observations from Gibraltar and
385 South-West Iceland. Int. J. Climatol. 17, 1433-1450. The NAO index data are
386 available from NCAR at www.cgd.ucar.edu/cas/catalog/climind/
387 Jones, P. D., and A. Moberg (2003), Hemispheric and Large- Scale Surface Air
388 Temperature Variations: An Extensive Revision and an Update to 2001, J. Clim.,
389 16, 206–23;
390 Jungclaus, J. H., H. Haak, M. Latif, U. Mikolajewicz (2005), Arctic–North Atlantic
391 Interactions and Multidecadal Variability of the Meridional Overturning
392 Circulation, J. Clim., pp. 4013-4030.
393 Kerr, R. A., A North Atlantic Climate Pacemaker for the Centuries (2000), *Science* 16 Vol.
394 288 no. 5473 pp. 1984-1985. DOI: 10.1126/science.288.5473.1984
395 Meehl, Gerald A., W.M. Washington, C. M. Ammann, J. M. Arblaster, T. M. L. Wigley, C.
396 Tebaldi (2004). "Combinations of Natural and Anthropogenic Forcings in
397 Twentieth-Century Climate". J. Clim. 17: 3721–7. DOI:10.1175/1520-
398 0442(2004)017%3C3721:CONAAF%3E2.0.CO;2. ISSN 1520-0442.
399 Menne, M.J., and C. N. Williams (2005), Detection of undocumented change points using
400 multiple test statistics and reference series, J. Clim., 18, 4271-4286. The NOAA
401 average land temperature estimate can be downloaded at
402 ftp.ncdc.noaa.gov/pub/data/anomalies/monthly.land.90S.90N.df_1901-
403 2000mean.dat
404 Muller, R. A. and G. MacDonald, (2002), Ice Ages and Astronomical Causes: data, spectral
405 analysis, and models. 337 p. ISBN 978-3540437796. Springer/Praxis Publishing.

406 Munnich, M. Latif, S. Venzke, E. Maier-Reimer (1998), Decadal Oscillations in a
407 Simple Coupled Model, J. Clim. vol 11, 3309-3319.
408 NOAA (2011). We used the Nino 3.4 data available from the Earth System Research
409 Laboratory, Physical Sciences Division, at:
410 www.esrl.noaa.gov/psd/data/correlation/nina34.data
411 and from the NOAA Climate Prediction Center at:
412 www.cpc.ncep.noaa.gov/data/indices/wksst.for
413 Rohde, R., D. Brillinger, J. Curry, D. Groom, R. Jacobsen, R.A. Muller, S. Perlmutter, A.
414 Rosenfeld, C. Wickham, J. Wurtele (2011), Berkeley Earth Temperature Averaging
415 Process, submitted to Econometrics.
416 Scafetta, N. (2010), Empirical evidence for a celestial origin of the climate oscillations and
417 its implications. Journal of Atmospheric and Solar-Terrestrial Physics,
418 doi:10.1016/j.jastp.2010.04.015
419 Schlesinger, M. E., and Ramankutty, N. (1994), An Oscillation in the global climate system
420 of period 65-70 years, *Nature* **367**, 723 - 726); doi:10.1038/367723a0
421 Sévellec, F. and A. V. Fedorov (2010), Excitation of SST anomalies in the eastern
422 equatorial Pacific by oceanic optimal perturbations, accepted in J. Mar. Res.
423 Sévellec, F., T. Huck, M. Ben Jelloul and J. Vialard (2009), Non-normal multidecadal
424 response of the thermohaline circulation induced by optimal surface salinity
425 perturbations, J. Phys. Oceanogr., 39, 852-872.
426 Thompson, D. W. J., and J. M. Wallace (1998), The Arctic Oscillation signature in the
427 wintertime geopotential height and temperature fields. Geophys. Res. Lett., 25, No.
428 9, 1297-1300

429 Trenberth, K.E., J. M. Caron, D. P. Stepaniak, and S. Worley (2002), Evolution of El
430 Niño–Southern Oscillation and global atmospheric surface temperatures
431 J.Geophys.Res., 107, D8, doi:10.1029/2000JD000298, 2002
432 Trenberth & Shea (2006), Geophysical Research Letters 33, L12704,
433 doi:10.1029/2006GL026894. Updated index available from NOAA at:
434 www.esrl.noaa.gov/psd/data/correlation/amon.us.long.data
435 and www.cdc.noaa.gov/Timeseries/AMO/
436
437 Zhang, R., and T. L. Delworth (2007), Impact of the Atlantic Multidecadal Oscillation on
438 North Pacific climate variability. Geophysical Research Letters, 34, L23708,
439 doi:10.1029/2007GL031601.
440 Zhang, R., T. L. Delworth, and I. Held (2007), Can the Atlantic Ocean drive the observed
441 multidecadal variability in Northern Hemisphere mean temperature? Geophysical
442 Research Letters, 34, L02709, doi:10.1029/2006GL028683
443
444
445 **FIGURE CAPTIONS**
446
447 **Figure 1.** Global land temperature estimates T_{avg}, smoothed by a 12-month moving
448 average. The temperature anomaly is the difference between the estimated temperature and
449 the mean in the period 1950-1980 for each temperature series. Note the similarity of many
450 of the short-term fluctuations with periods 2-15 years. The Berkeley Earth data were
451 randomly chosen from 30,964 sites that were not used by the other groups.
452

453 **Figure 2.** The AMO index. The pattern is dominated by the 65-70 year multidecadal
454 oscillation that gave the index its name. In this paper, we are more interested in the short-
455 term 2-15 year variations that are evident in the 12-month smoothed curve.
456
457 **Figure 3.** Decadal fluctuations in surface land temperature estimates and in oceanic
458 indices. The long-term variability was suppressed by removing the least-squares fit 5th
459 order polynomial from each curve. (A) shows the 12-month smoothed land surface
460 temperature estimates from the four groups. The decadal variations are very similar to
461 each other. The Berkeley Earth data were derived from 2000 sites chosen randomly from a
462 set of 30964 that did not include any of the sites from the other groups. (B) shows the
463 AMO index compared to Tavg, the average of the four land estimates. (C) shows the
464 ENSO index compared to the average of the four land estimates. (D) shows the AMO and
465 ENSO directly. Note that the AMO agreement in (b) is qualitatively stronger than the
466 ENSO agreement in (c).
467
468 **Figure 4** . Decadal correlations of the Berkeley Earth land temperature estimates Tavg with
469 the (a) AMO index, (b) ENSO index, (c) PDO index, and (d) NAO index. The strongest
470 correlation observed, 0.65 ± 0.04, is with the AMO.
471
472 **Figure 5**. (a) shows the pre-whitened AMO and PDO indices plotted together vs time. It
473 can be seen that PDO leads AMO by about 2.5 years. (b) shows the correlation of AMO
474 and PDO vs lag. The periodicity of the correlation (4.5 cycles in 40 years of lag) is a result
475 of the apparent presence of a 9 year cycle in both.
476

Figure 6. Correlation maps of the filtered AMO and ENSO time series with similarly filtered temperature time series taken from the Earth's surface temperature map constructed by the NOAA group. Colors show the degree of correlation at each location. AMO is observed to have positive or neutral correlation almost everywhere, while ENSO shows both strong positive and negative correlations.

Figure 7. Spectral power in the (a) Atlantic Multidecadal Oscillation and in (b) the Pacific Decadal Oscillation. The low frequency oscillations (< 0.06/yr) have been suppressed by the subtraction of a best-fit 5th order polynomial from each time series prior to calculation of the spectrum; similarly, a 12-month running average eliminated high frequency (e.g. monthly) fluctuations. A strong peak is observed in the AMO at 0.110 ± 0.005 cycles/year, corresponding to a period of 9.1 ± 0.4 years, at the 98.3% confidence level. The maximum peak in the PDO occurs at a similar frequency, 0.111 ± 0.006, although with a confidence level of 94%.